第 31 卷第 12 期 无 机 化 学 学 报 Vol.31 No.12
2015 年 12 月 CHINESE JOURNAL OF INORGANIC CHEMISTRY 2401-2410

共聚物模板辅助合成高倍率性能多孔 Li_2FeSiO_4@C/CNTs 纳米复合正极材料

苟 蕾 赵 坤 毛一洋 谢 荣 樊小勇 李东林* 马守龙 田 苗
(长安大学材料科学与工程学院,新能源材料与器件研究所,西安 710061)

摘要: 通过溶胶–凝胶法制备了 Li_2FeSiO_4@C/CNTs(LFS@C/CNTs)纳米复合材料,其中三嵌段共聚物 P123 用作结构导向剂和碳源,碳纳米管作为导电线提高材料的导电性。LFS@C/CNTs 不仅具有海绵状纳米孔,能够与电解液充分接触改善锂离子的传输路径,同时由非晶碳和碳纳米管构成的三维桥联导电网络利于电子的快速传递,提高了材料大电流充放电能力和循环稳定性。复合后的 LFS@C/CNTs 的高倍率性能相比 LFS@C 明显提高, 当 CNTs 的掺量为 4%,电压窗口为 1.5~4.5 V,0.1C 电流密度下放电比容量为 182 mAh·g^{-1}。在 10C 经 70 次循环后该材料的放电比容量能保持在 117 mAh·g^{-1},是 LFS@C 放电比容量(55 mAh·g^{-1})的两倍。

关键词: Li_2FeSiO_4; 复合材料; 碳纳米管; 锂离子电池; 倍率性能
中图分类号: O611.3 **文献标识码**: A **文章编号**: 1001-4861(2015)12-2401-10
DOI:10.11862/CJIC.2015.286

Copolymer Template-Assisted Synthesis of Porous Li_2FeSiO_4@C/CNTs Nanocomposite as Cathode Material with High Rate Capability

GOU Lei ZHAO Kun MAO Yi-Yang XIE Rong FAN Xiao-Yong
LI Dong-Lin* MA Shou-Long TIAN Miao
(*New Energy Materials and Device Group, School of Materials Science and Engineering, Changan University, Xian,* 710061, *China*)

Abstract: Li_2FeSiO_4@C/CNTs (LFS@C/CNTs) nanocomposite was synthesized by a sol-gel method. A triblock copolymer P123 was used as the direction agent for nanopores and carbon source, and carbon nanotubes were used as conductive wires to further increase the conductivity of the material. The resulting LFS@C/CNTs nanocomposite possesses not only a nanoporous sponge-like structure for improving Li-ions transport by means of liquid electrolyte, but also a 3D self-bridged conduction hybrid network consisted of amorphous carbon coating and graphitized CNTs for electron fast transport that ultimately improves the high rate capability and cycling performance. As a result, the porous LFS@C/CNTs nanocomposite compared with nanoporous LFS@C exhibits a remarkable improvement in high-rate capability. The LFS@C/CNTs nanocomposite with 4wt% of CNTs delivers a specific discharge capacity of approximately 182 mAh·g^{-1} at 0.1C in the voltage window of 1.5~4.5 V, and the specific discharge capacity at 10C after 70 cycles maintains at 117 mA·h·g^{-1}, which is more than two times that of LFS@C (55 mAh·g^{-1}) as a cathode material for high power lithium ion battery.

Key words: Li_2FeSiO_4; composite materials; carbon nanotube; lithium ion battery; rate performance

收稿日期:2015-07-10。收修改稿日期:2015-08-14。
国家自然科学基金(No.21073021,21473014,21103013),教育部科技创新工程重大项目培育资金(No.708084),中央高校基础研究经费(No.0009-2014G1311085)资助项目。
*通讯联系人。E-mail:donglinli@hotmail.com

0 Introduction

Since Nytén et al.[1] reported the electrochemical properties of the polyanion compound Li_2FeSiO_4(LFS) in 2005, many works have been focused on the LFS as a potential cathode material for next-generation lithium ion batteries[2-6]. The LFS possesses many advantages, such as low cost, environmental friendliness, high safety and chemical stability. In particular, the LFS crystal has the possibility to reversibly extract or insert two lithium ions (corresponding to the Fe^{2+}/Fe^{3+} and Fe^{3+}/Fe^{4+} redoxs) from the host structure and thus delivers a theoretical capacity of 333 mAh·g^{-1}. However, the LFS suffers from a problem of poor electronic conductivity and slow lithium ion diffusion rate, leading to a poor rate-performance[7-8]. In addition, it is difficult to synthesize high-purity LFS, because SiO_2 impurity is always presented and would cause a loss of the apparent capacity or poor rate-performance[9].

Many efforts have been made to improve the rate performance of the LFS cathode material in virtue of reducing the particle size to nanometer scale to shorten the lithium ion diffusion distance and to remarkably increase the effectively active surface area[9-13], coating the particle surface with a conductive phase to improve the electron transport rate[3,9-13] and introducing appropriate porosity to facilitate the electrolyte irrigation[9-14] as well as cationic doping to enhance the electronic conductivity[4-5,15-16]. By controlling the crystallization and the composition of materials, a smaller amount of mixed valence Fe_7SiO_{10} nanocrystals intergrow with LFS nanocrystals instead of glassy SiO_2, thus improving the rate charge/discharge performance of LFS cathode[9]. Among the above modifying methods, the *in situ* coating of carbon on the surface of the LFS particles is one of the preferred approaches to enhance the electrochemical performance of the insu-lating cathode due to its simple synthesis process[12,17]. Usually, the introduced amorphous carbon is coated around the active particles, forming LFS@C composite particles to improve the electrical conductivity of the cathode at the nanoscale. However, micrometer conductivity is limited by the electrical contact between the particles, making it difficult to improve the high rate performance of the Li_2FeSiO_4 during high rate charge-discharge process, which is extremely important to power electric vehicles (EVs) and hybrid electric vehicles (PHEVs). As a conductive phase, one-dimensional (1D) CNTs have been successfully employed in the modification of $LiFePO_4$, $Li_3V_2(PO_4)_3$ and other cathode materials[18-23] in which the high-rate performance is significantly improved because of the decreased charge transfer impedance between the particles. Peng et al.[24] exhibit that the CNTs modified bulk LiFS@C composite fabricated via a sol-gel method can deliver a higher specific capacity, but no apparent improvement is seen on high-rate performance, while the LFS coating on CNTs[25] and CNT @LFS arrays[26] shows an improved high-rate performance. Although there are many reports on the LFS materials, the rate performance and micro-nano structures of the LFS is neither controlled nor well understood.

In this paper, we demonstrate a facile synthesis of nanoporous double nano-carbon decorated LFS nanocomposites that achieve ultrahigh rate capability. We use the amphiphilic triblock copolymers P123 as a structure directing agent for nanopores to control LFS@C particles at the nanoscale and to realize an efficient electrolyte infiltration.

The CNTs, *in situ* added into the LFS precursor, act as 1D conductive bridges to connect the LiFS@C nanoparticles together to facilitate the electron transfer and reduce the electrochemical polarization at high rates. Owing to the synergistic effects of the nano-size particles and CNTs conduction network, as well as sufficient nanopores, the LFS@C/CNTs nanocomposite with 4wt% CNTs content delivers the superior electrochemical performance, and the discharge specific capacity reaches up to 117 mAh·g^{-1} even at the current rate of 10 C and the capacity retention at 10C rate is up to 64% compared with the capacity of the material at 0.1C rate and room

temperature.

1 Experimental

1.1 Chemicals

All the agents used are analytical grade. The CNTs were purchased from Nano Port (Shenzhen) Co., Ltd. The CNTs were subject to some pretreatment to remove any impurities and to graft some polar groups like -OH and -COOH on CNTs surface to make them more dispersible in polar solvent.

1.2 Synthesis of porous Li_2FeSiO_4@C/CNTs nanocomposite

The LFS sol was synthesized via a sol-gel method. The stoichiometric ratio of Li∶Fe∶Si used in the precursor was 2.1∶1∶1 (with little excess content of Li). In a typical synthesis, 1 g triblock copolymer Pluronic P123 ($EO_{20}PO_{70}EO_{20}$) was dissolved in an absolute alcohol under vigorous magnetic stirring at 35 ℃ for 3 h. Then the alcohol solution of tetraethyl orthosilicate (TEOS) was added into the P123 solution, resulting in a homogeneous and colorless mixture, to which a mixed alcohol solution containing lithium acetate and ferric nitrate was added, a transparent sol was obtained by stirring for another 3 h. Subsequently, an acid-treated CNTs suspension, which was prepared by dispersing a certain amount of the acid-treated CNTs in an absolute alcohol under ultrasonication for 3 h, was added into the LFS-P123 sol under a vigorous stirring. After aging at room temperature for a week, a solid gel sample was formed which was then calcined in a horizontal quartz tube oven under flowing argon gas. First the sample was heated at a rate of 2 ℃·min^{-1} to obtain a constant temperature of 400 ℃ for 4 h and then the temperature was increased at the same rate to plateau at 650 ℃ for another 10 h. For comparison, the LFS@C composite was synthesized via the same process without adding CNTs.

1.3 Materials characterization

Powder X-ray diffraction (Bruker D8A A25 X, Germany) using Cu $K\alpha_1$ radiation (λ=0.154 056 nm) was used to determine the crystalline phase of the synthesized material. The morphology and nanostructure of the synthesized powders were examined with field emission scanning electron microscope (FESEM, Hitachi S-4800) and transmission electronic microscopy (TEM, FEI Tecncnai F30) technologies. The carbon contents in the composites were measured by thermal gravimetric analysis (TGA, TA Q50).

1.4 Electrochemical measurements

The electrochemical characterization was performed using coin-type cells, consisting of a lithium metal anode and a LFS@C/CNTs nanocomposite cathode that were separated by a Celgard 2400 microporous film. 1 mol·L^{-1} $LiPF_6$ in ethylene carbonate/dimethyl carbonate (1∶1,*V*/*V*) was used as the electrolyte. For cathode fabrication, the synthesized LFS@C/CNTs composite was mixed well with the carbon black and polyvinylidene difluoride (PVDF) with a weight ratio of 80∶15∶5. After the composite was coated on an aluminum foil, which served as a current collector, the cathode film was dried at 100 ℃ for 16 h in an oven. The assembly of the cells was carried out in an Ar-filled glove box. The cells were galvanostatically charged and discharged between 1.5 V and 4.5 V vs. Li/Li^+ on a battery test system (Neware CT-3008W-S4, China). CV was tested with an electrochemical workstation (Versa STAT Princeton). All the electrochemical tests were carried out at room temperature, and the charge/discharge specific capacities mentioned in this paper were calculated on the mass of pure LFS by excluding the weight of carbon and CNTs.

2 Results and discussion

2.1 Characterization of the products

In order to identify the effects of CNTs on the electrochemical properties of the LFS electrode, the nanoporous LFS@C (without CNTs) nanocomposite was also prepared using the same procedure as the nanoporous LFS@C/CNTs. Fig.1 shows XRD patterns of the as-prepared LFS@C/CNTs and LFS@C nanocomposites. There are no obvious differences between the two XRD patterns. The main diffraction peaks of both samples are in good agreement with the

monoclinic structure of a space group of $P2_1/n$ according to the results reported by Nishimura et al. ($P2_1/n$, a =0.822 898 nm, b =0.502 002 nm, c = 0.823 335 nm, and β=99.202 7°)[27]. There exists a little metallic iron (Fe) impurity in both samples, which might be caused by the over-reduction during the sintering process[22]. The average crystallite size of the LFS in the LFS@C/CNTs and LFS@C materials is (8± 4) nm, as estimated from the widths of major diffraction peaks of (111), (202), and (020) by Scherrers formula.

The morphology and nanostructure of the materials were identified by FESEM and TEM techniques. Fig.2a shows the FESEM images of the LFS@C sample. The short wormlike rods approximately 5 nm in diameter and approximately 20 nm in length are loosely packed to form mesoporous sponge-like micrometer-sized particles in the LFS@C sample, as reported previously[9]. The formation of the wormlike rods may be templated from the columnar micelles of copolymer P123 which is usually used to synthesize ordered mesoporous materials[28-29]. The columnar micelles of nonionic triblock copolymer P123 are

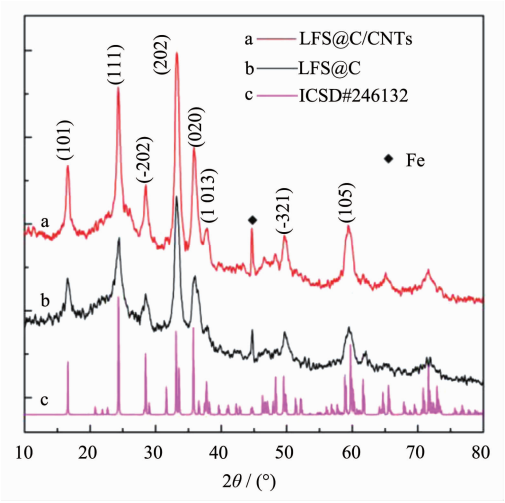

Fig.1 XRD patterns of (a) LFS@C/CNTs and (b) LFS@C nanocomposites, (c) ICSD#246132 pattern of LFS

intersected with each other and carbonized into an amorphous carbon phase. In addition, the nanoparticles approximately 5~20 nm in diameter are also observed. The amorphous carbon coats around the LFS nanocrystals to form a sponge-like LFS@C nanocomposite, which is further confirmed by the HRTEM observation.

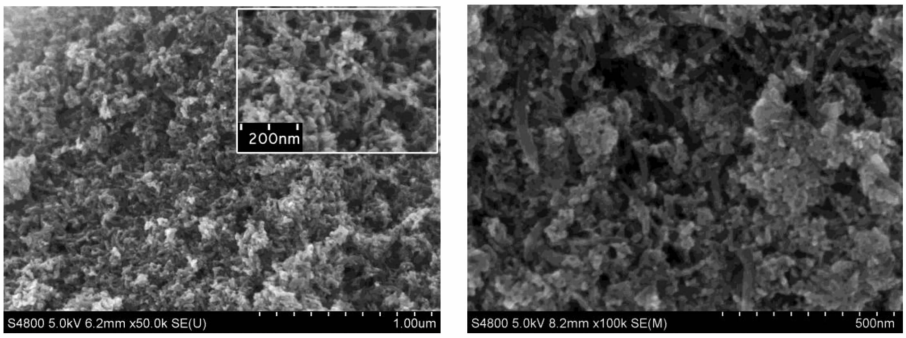

Fig.2 FESEM images of the (a) LFS@C and (b) LFS@C/CNTs nanocomposites

Fig.3a shows a HRTEM image of LFS@C thin flake. The HRTEM image of the LFS@C nanocomposite reveals the well crystallized nature of LFS, and the regular interplanar spacing of 0.267 nm could be ascribed to the (202) planes of monoclinic LFS. After carefully examining the samples under HRTEM, the amorphous carbon layer is not uniform in size, ranging from 1~6 nm in thickness, even bulk carbon is observed. Thus, some of the LFS nanocrystals are not completely coated by amorphous carbon. The amorphous carbon content is around 9.5wt% according to TGA measurements.

After introducing 4% CNTs into the precursor sol of the materials, the CNTs are clearly observed (Fig. 2b). The CNT in the LFS@C/CNTs has a smooth outer surface with diameters around 20 ~40 nm and submicrometers in length. The nanocomposite exhibits nanoporous structures including the disordered

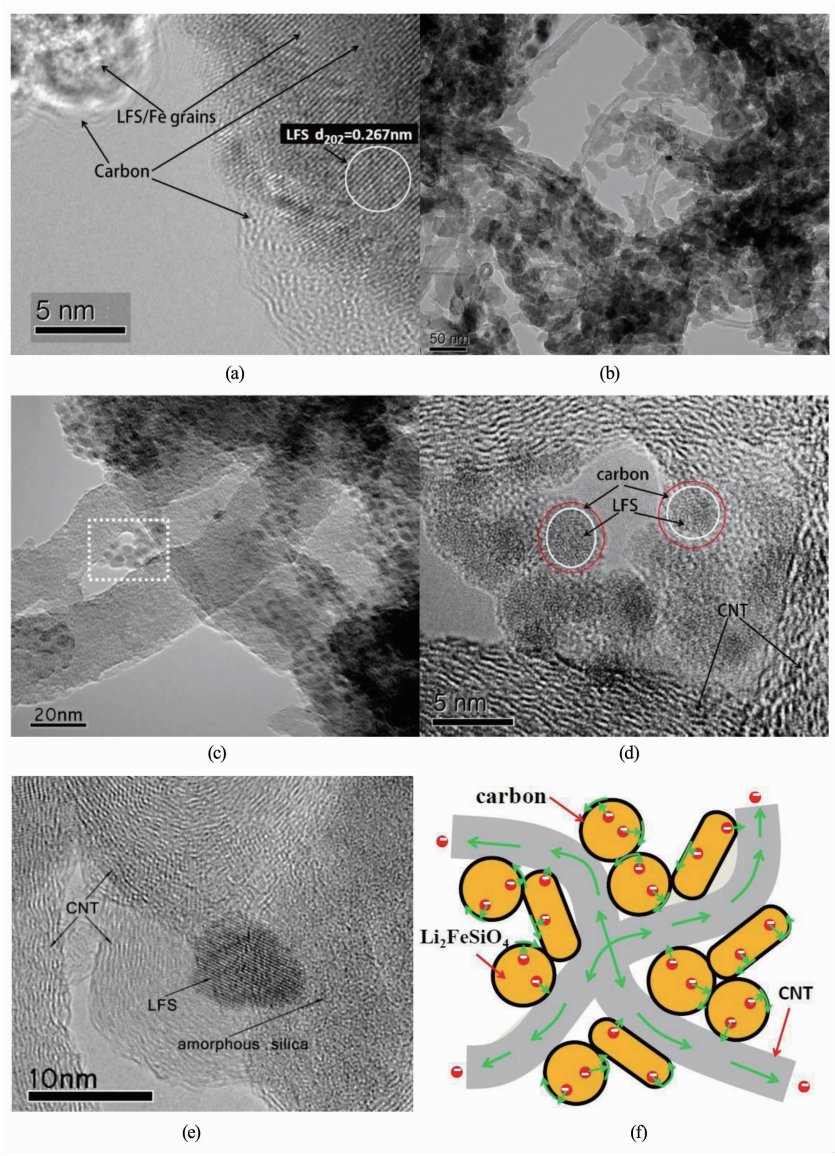

(a) HRTEM image of LFS@C; (b, c) TEM images of LFS@C/CNTs; (d, e) HRTEM image of LFS@C/CNTs; (f) Nanostructure and electron transport model

Fig.3　TEM images of the materials

mesopores templated from P123 and irregular larger nanopores derived from intersected CNTs. The isolated nanoparticles with an average size of 5~20 nm are observed on the surface of CNTs, and most of the nanoparticles are further connected by 1D CNTs. The self-bridged network structure that connects the nanoparticles is further confirmed by transmission electron microscopy (TEM). Fig.3b and 3c are TEM images of the LFS@C/CNTs nanocomposite and they clearly show that uniform nanoparticles with a particle size of 5~20 nm anchor on the CNTs which serve as bridges for the electron transport between the nanoparticles. The HRTEM images reveal that the nanoparticle is a core-shell structure consisting of a LFS core approximately 5 nm in diameter and an amorphous carbon shell approximately 1 nm in thickness, as shown in Fig.3d. Most of the nanoparticles are LFS@C core-shell structures. In addition, a tiny amount of glassy SiO_2 exists in the samples (Fig.3e). By comparing this with the HRTEM image of original CNTs, the amorphous carbon shells are coated around the LFS crystals along with CNTs

together forming a self-bridged 3D conduction hybrid network. The CNTs act as the faster electron conduction wires between the LFS@C nanoparticles, resulting in a double nano-carbon 3D network consisting of amorphous carbon and CNTs, as shown in Fig.3e. The net carbon content is around 12.8wt% according to TGA measurements. Such a LFS@C/CNTs nanostructure possesses not only nanoporous sponge-like structure for improving Li-ions transport by means of liquid electrolyte, but also a double nano-carbon 3D self-bridged network for electron fast transport that ultimately improves the high rate capability and cycling performance.

2.2 Electrochemical characteristics

The galvanostatic charge/discharge profiles of the LFS@C and LFS@C/CNTs samples between 1.5 and 4.5 V at 0.1C and at room temperature for the first, second, fifth and tenth cycles are shown in Fig.4. There are no apparent differences between two profiles at lower rates. In the charge curves, there exist a main plateau around 2.8 V and a short plateau at 4.3 V for both samples. The LFS@C/CNTs nanocomposite delivers an initial discharge capacity of 205 $mAh \cdot g^{-1}$ with slight capacity fade in the consecutive cycles. The discharge capacities at the 2nd, 5th and 10th cycles are 198, 193 and 186 $mAh \cdot g^{-1}$, respectively (Fig.4a). Considering a tiny amount of metallic Fe content, the LFS would deliver higher capacities than the measured data. The LFS@C delivers a higher initial discharge capacity of 216 $mAh \cdot g^{-1}$ (Fig.4b), however, the capacity drops rapidly in the early cycles. The capacity retention in the tenth cycle is only 83% while that of the LFS@C/CNTs nanocomposite is up to 91% compared with the initial discharge capacity. In order to identify this data, we carefully measured cyclic voltammogram (CV) behavior of the LFS@C/CNTs sample for the second cycles in the potential window of 1.5~4.8 V vs Li^+/Li. As can be seen in Fig.4c, it shows a pair of anodic (3.0 V) and cathodic (2.6 V) peaks in the second cycle. The peak around 3.0 V in the charge process presents that the first lithium ion is extracted. Unlike sharp peaks in the CV curve for $Li_3V_2(PO_4)_3$ cathode[30], the LFS cathode exhibits diffusive saddle-like humps. In addition, a pair of weak anodic (4.2 V) and cathodic (1.8 V) humps is observed, which is in agreement with the short plateau around 4.2 V in the charge curve. This weak peak should contribute a small quantity of capacity to the cell. The LFS@C sample exhibits a similar CV behavior. Taking into account the previous report[3], a plausible interpretation of the higher discharge capacity is that a small portion of secondary ion may extract from up 4.1 V in the charge process.

The CNT-amorphous carbon conductive hybrid network can significantly improve rate capability of the LFS cathode at high rates. The galvanostatic charge/discharge profiles of the LFS@C and LFS@C/CNTs nanocomposites at different rates are shown in Fig.5. As the current rate (C-rate) increases, the plateau voltage at approximately 2.8 V for the LFS@C sample declines rapidly toward lower potential, and becomes gradually undistinguished due to the increased

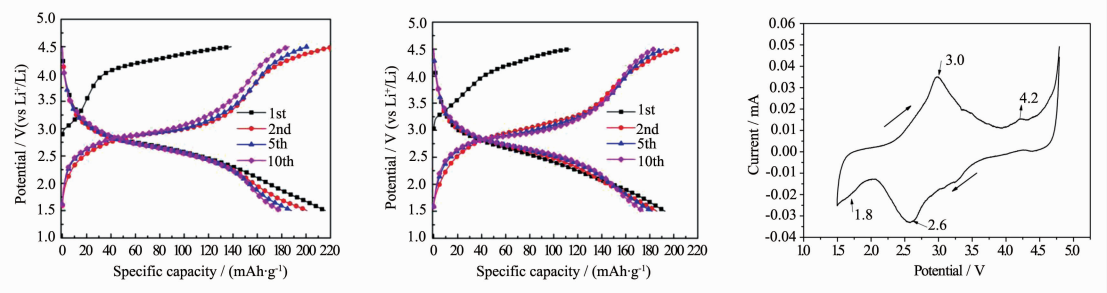

Fig.4 Electrochemical properties of the materials. Charge/discharge voltage profiles of the 1st, 2nd, 5th and 10th cycles for the (a) LFS@C/CNTs and (b) LFS@C nanocomposites recorded at 0.1C (1C=166 $mA \cdot g^{-1}$) and room temperature between 1.5 and 4.5 V; (c) Cyclic voltarmmetry curve at a scan rate of 0.05 $mV \cdot s^{-1}$ in the potential range from 4.8~1.5 vs Li/Li^+

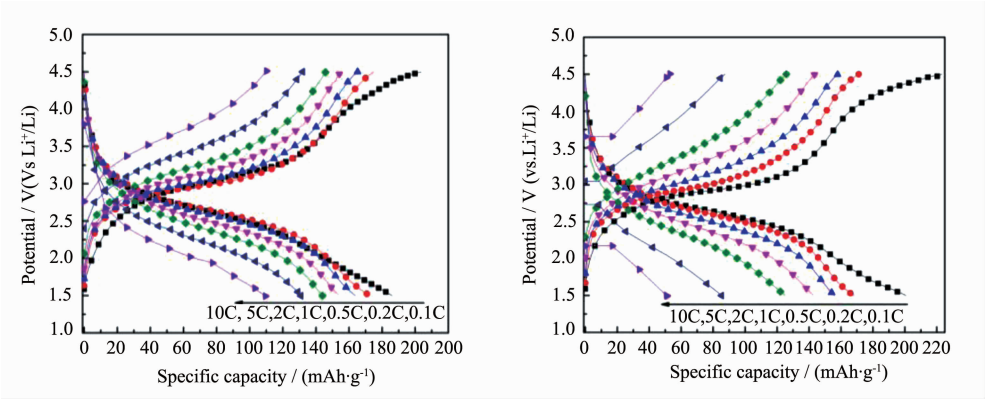

Fig.5　Charge/discharge voltage profiles of the (a) LFS@C/CNTs and (b) LFS@C samples at different rates in the voltage range of 1.5~4.5 V

cell polarization at high rates. By contrast, the 2.8 V discharge plateau of the LFS@C/CNTs is still distinguished even at 10C while that of the LFS@C becomes a slope line. These results show that the LFS@C/CNTs is remarkably improved by means of the CNT-amorphous carbon hybrid conduction network, leading to enhanced high-rate performance. This conclusion is further confirmed by the cycling performances of the LFS@C and LFS@C/CNTs electrodes at different C-rates.

As shown in Fig.6a, the capacity of the LFS@C/CNTs nanocomposite shows a relatively slower decay during the C-rates test than that of the LFS@C sample. As a result, the LFS@C/CNTs nanocomposite delivers a higher capacity than the LFS@C sample at high rates. For example, the LFS@C/CNTs nanocomposite delivers a specific discharge capacity of approximately 182 mAh·g^{-1} at 0.1 C in the voltage window of 1.5 ~4.5 V and the specific discharge capacity at 10 C after 70 cycles maintains at 117 mA·h·g^{-1}, which is more than two times that of LFS@C. The LFS@C/CNTs electrode shows remarkably improved rate capability and the discharge capacity retention reaches up to 64% at 10C while that of LFS@C is only 26% compared to the discharge capacity of the 2nd cycle at 0.1C. The cycle coulombic efficiency of both samples remains almost 100%, demonstrating that it has good reversibility and structural integrity during cycling at every current rate except for several early cycles. The decay of the capacity and lower coulomic efficiency in the several early cycles might be explained by the side-reaction in the initial cycles leading to the loss of reversible lithium ions. Although the capacity of the present materials is lower than the previous data measured in the voltage window of 1.5~4.8 V[7], the present nanoporous LFS@C/CNTs nanocomposite exhibits indeed a significant improvement in rate capability, in particular, the 2.8 V discharge plateau is distinguished at a high rate, which renders the battery with a higher

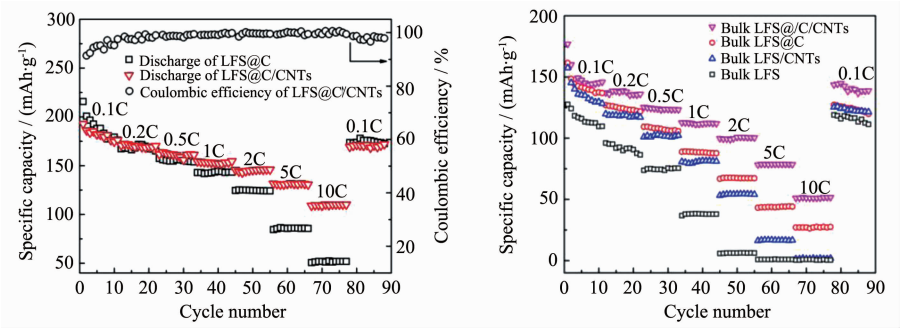

(a) Nanoporous LFS@C and LFS @C/CNTs nanocomposites, (b) bulk LFS, LFS@C, LFS/CNTs and LFS@C/CNTs nanocomposites

Fig.6　Discharge cycling performances of the materials at different rates in the voltage window of 1.5~4.5 V

energy density. The slightly lower capacity may be associated with a tiny amount of amorphous SiO_2 and different voltage windows.

Fig.7 represents AC impedance spectra of LFS@C and LFS@C/CNTs and fitting curves showing calculated results from equivalent circuit. Each Nyquist plot is composed of a depressed semicircle and a straight line. The semicircle in the middle frequency range is attributed to the charge transfer process, and the diameter of the semicircle is approximately equal to the charge transfer resistance (R_{ct}). The straight line in the low frequency is associated with lithium ion diffusion in LFS. According to the fitting results, the charge tansfer resistants for LFS@C/CNTs and LFS@C are 64 Ω and 100 Ω, respectively. The smaller semicircle diameter along with a smaller charge transfer resistance value of LFS@C/CNTs reflects a lower charge transfer impedance within the LFS@C/CNTs cathode, showing a good coherence with the rate capacity results showed in Fig.6.

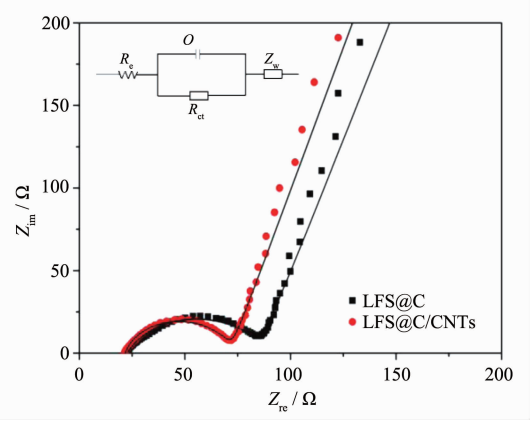

Fig.7 AC impedance spectroscopies of LFS@C and LFS@C/CNT composites and fitting curves showing calculated results from equivalent circuit

2.3 Control experiments

To further confirm the effects of a single carbon coating layer or CNTs on rate performance of the LFS cathode, we prepared bulk LFS, LFS@C, LFS/CNTs, LFS@C/CNTs nanomaterials by using a similar process in the absence of the P123 template, thus the effects of nanopores on lithium ion transporting at high rates of different cathodes could be ignored due to free of a meso-porosity. The rate capabilities of all four samples are evaluated at the same measurement conditions (Fig.6b). The results clearly show that the bulk LFS@C/CNTs exhibits the best high-rate capability, and the bulk LFS@C shows better high-rate capability than the bulk LFS/CNTs, while the bulk pristine LFS shows poor high-rate performance. For example, at a high rate of 5C, the capacity retention of the bulk LFS@C/CNTs is about 51%, which is significantly larger than 35% of the bulk LFS/C, 17% of the bulk LFS/CNTs, and 0% of the bulk pristine LFS. Upon further increasing the current rate to 10 C, the discharge capacities of bulk LFS@C/CNTs and bulk LFS@C drop from 75 $mAh \cdot g^{-1}$ and 50 $mAh \cdot g^{-1}$ at 5 C to 50 $mAh \cdot g^{-1}$ and 25 $mAhg^{-1}$, respectively, while those of the LFS and LFS/CNTs drop dramatically to 0 $mAh \cdot g^{-1}$ at 10 C. For the bulk samples, the LFS@C is better than LFS/CNTs, indicating the amorphous carbon coating layer is necessary for high-rate capacity retention. The amorphous carbon layer residing around LFS crystallites with CNTs together consists of a 3D self-bridged conduction network for electron transport.

Although a tiny amount of metallic Fe is detected in LFS@C and LFES@C/CNTs samples, which can improving the rate capability of LFS electrode [31], the relative intensity of the metallic Fe in the XRD patterns is similar for both samples.

Thus the effects of the metallic Fe on electrochemical properties are similar. The sole difference between both electrodes is the CNTs. According to the rate and cycling test data of nanoporous samples and nanostructure observations, it can be deduced that both nano-porosity and double nano-carbon 3D self-bridged networks play a synergistic role on improving the rate performance of LFS@C/CNTs electrodes. Firstly, the sponge-like LFS@C particle can facilitate electrolyte permeation into the micrometer sized particle, thus providing direct access and reservoirs for impregnating electrolyte into micrometer LFS@C particles as well as more interface area between the electrode and the electrolyte that improve Li^+ ion transport rate in the

cathode. Secondly, the double nano-carbon 3D self-bridged network play a crucial role of transporting electrons during charge-discharge process. Because the rate performance of the LFS cathode is significantly restricted by sluggish kinetics of electron transport in the interior of the LFS crystallites which is due to its poor electrical conductivity, at approximately 10^{-14} S·cm^{-1}, single amorphous carbon layer or CNTs, cannot completely fulfil electron transport at high-rates. The diffusion flux of electrons in the LFS nanocrystal-amorphous carbon core-shell structure is relatively higher than that of LFS/CNTs, due to its larger contact area (2-D contact) between active crystallites and the conductive phase than that of the LFS/CNTs, and the electron transport kinetics in the LFS@C is better than the LFS/CNTs (0 or 1D contact area). Moreover, since the disordered nanopores (pores between nanoparticles) result in poor electrical contact between the loose packed LFS@C nanoparticles due to contraction-expansion cycles during the charge-discharge cycles, electron transport is limited by the interface of the LFS@C nanoparticles. For LFS@C/CNTs, electrons produced during electrochemical reaction transfer fast to the amorphous 2-D carbon layer, then the 1-D CNTs approximately sub-micrometers in length serve as a bridge between LFS@C nanoparticles anchored on them for the electron transport from the LFS@C nanoparticles to the CNTs, as illustrated in Fig.3f. Thus the major role of the CNTs is to construct a highly efficient electron conduction network to improve the electrical contact between the LFS@C particles and hence enhance the high rate performance of the materials, even if a tiny of insulating SiO_2 phase with a size of 2~5 nm exists in the cathode. Compared with the previous works [25-26], the present LFS cathode material contains a smaller amount CNTs which can improve the rate capability of insulating LFS cathode by a simple sol-gel method, thus making the apparent capacity of the cathode higher. Also, the present work indicates that it is difficult to improve the rate performance of poorly conductive LFS only through constructing a nanoporous structure for enhancing Li^+ ions transport. By contrast, the NASICON-type Li_3V_2 $(PO_4)_3$ possesses higher electrical conductivity [32-33], which is a macro-porous structure that can remarkably improve its high rate performance[34]. The present results indicate that the main kinetics limit for the Li_2FeSiO_4 material may be its electronic conductivity during a high rate charge-discharge process.

3 Conclusions

In summary, we have synthesized nanoporous Li_2FeSiO_4@C/CNTs nanocomposites with 3-D conduction hybrid networks consisting of amorphous carbon coating and graphitized CNTs to improve the electrochemical properties of Li_2FeSiO_4 cathode materials by a sol-gel procedure. Compared with single-carbon decorated LFS@C, the designed LFS@C/CNTs exhibits the improved high-rate capability (about 64% capacity retention at an ultrahigh rate of up to 10C). These properties may result from the synergistic effect of the amorphous carbon coating and the graphitized conductive CNTs for electron transport as well as nanoporosity for lithium ion transport. Whereas the amorphous carbon layer is coated on all LFS nanoparticles and plays a major role on promoting the ability of electron transport on the interface of LFS nanocrystals and stabilizing the interface of the LFS nanoparticles, the CNTs decrease the internal resistance by wiring electronically all the LFS@C particles and forming an optimal three-dimensional conducting network in the entire electrode, hence further enhancing the high-rate performances of LFS. The present results indicate that the main kinetics limit for the LFS material may be its electronic conductivity during high-rate charge-discharge processes.

Acknowledgements: This work was financially supported by National Natural Science Foundation of China (No. 21073021, 21473014, 21103013), partially supported by Cultivation Fund of the Key Scientific and Technical Innovation Project, Ministry of Education of China (No.708084) and the Fundamental Research Funds for the Central Universities (No. 0009-2014G1311085).

References:

[1] Nytn A, Abouimrane A, Armand M, et al. *Electrochem. Commun.*, **2005**,**7**(2):156-160

[2] Huang X B, Li X, Wang H Y, et al. *Electrochim. Acta*, **2010**,**55**(24):7362-7366

[3] Wu X Z, Jiang X, Huo Q S, et al. *Electrochim. Acta*, **2012**,**80**:50-55

[4] Deng C, Zhang S, Zhao G S, et al. *J. Electrochem. Soc.*, **2013**,**160**:A1457-A1464

[5] Dominko R. *J. Power Sources*, **2008**,**184**(2):462-468

[6] Gong Z L, Li Y X, He G N, et al. *Electrochem. Solid-State Lett.*, **2008**,**11**(5):A60-A63

[7] Larsson P, Ahuja R, Nytn A, et al. *Electrochem. Commun.*, **2006**,**8**(5):797-800

[8] Bai J Y, Gong Z L, Lü D P, et al. *J. Mater. Chem.*, **2012**,**22**(24):12128-12132

[9] Li D L, Xie R, Tian M, et al. *J. Mater. Chem. A*, **2014**,**2:** 4375-4383

[10]Muraliganth T, Stroukoff K R, Manthiram A. *Chem. Mater.*, **2010**,**22**(20):5754-5761

[11]Choi D, Kumta P N. *J. Power Sources*, **2007**,**163**(2):1064-1069

[12]Delacourt C, Poizot P, Levasseur S, et al. *Solid-State Lett.*, **2006**,**9**(7):A352-A355

[13]Zhu H, Wu X, Zan L, et al. *Electrochim. Acta*, **2014**,**117**: 34-40

[14]Fan X Y, Li Y, Wang J J, et al. *J. Alloys Compd.*, **2010**,**493**:77-80

[15]Deng C, Zhang S, Yang S Y, et al. *J. Power Sources*, **2011**,**196**(1):386-392

[16]Hao H, Wang J B, Liu J L, et al. *J. Power Sources*, **2012**,**210**:397-401

[17]Dominko R, Conte D E, Hanzel D, et al. *J. Power Sources*, **2008**,**178**(2):842-847

[18]Bindumadhavan K, Srivastava S K, Mahanty S. *Chem. Comm.*, **2013**,**49**:1823-1825

[19]Tang M, Yuan A, Zhao H, Xu J. *J. Power Sources*, **2013**,**235**:5-13

[20]Li X, Qu M Z, Huai Y J, et al. *Electrochim. Acta*, **2010**,**55**(8):2978-2982

[21]Chen M, Du C Y, Song B, et al. *J. Power Sources*, **2013**,**223**:100-106

[22]Zhou H T, Mari-Ann E, Fride V B. *Solid State Ionics*, **2012**,**225**:585-589

[23]Sun X R, Li J J, Shi C S, et al. *J. Power Sources*, **2012**,**220**: 264-268

[24]Peng G, Zhang L L, Yang X L, et al. *J. Alloys Compd.*, **2013**,**570**(5):1-6

[25]Zhao Y, Li J, Wang N, et al. *J. Mater. Chem.*, **2012**,**22**: 18797-18800

[26]Zhou H, Lou F, Vullum P E, et al. *Nanotechnology*, **2013**,**24**(43):435703-435713

[27]Nishimura S I, Hayase S, Kanno R, et al. *J. Am. Chem. Soc.*, **2008**,**130**(40):13212-13213

[28]Li D, Zhou H, Honma I, et al. *Chem. Commun.*, **2005**,**41**: 5187-5189

[29]Li D, Zhou H, Honma I. *Nat. Mater.*, **2004**,**3**:65-72

[30]Luo Y, Xu X, Zhang Y, et al. *Adv. Energy Mater.*, **2014**,**14**: 400107

[31]Li D L, Yong H T H, Xie R, et al. *RSC Adv.*, **2014**,**4**: 35541-35545

[32]Huang H, Yin S C, Kerr T, et al. *Adv. Mater.*, **2002**,**14**(21): 1525-1528

[33]Yin S C, Grondey H, Strobel P, et al. *J. Am. Chem. Soc.*, **2003**,**125**(2):326-327

[34]Li D L, Xie R, Tian M, et al. *Nanoscale*, **2014**,**6**:3302-3308